Trans Indian Inst Met (2022) 75(4):1015–1030
https://doi.org/10.1007/s12666-022-02547-z

ORIGINAL ARTICLE

Newer Developments in Aluminium Alloys Through Ordered Precipitates and Segregation of Transition Elements

Ujjval Bansal[1] · Kamanio Chattopadhyay[1]

Received: 30 November 2021 / Accepted: 30 January 2022 / Published online: 9 March 2022

Abstract Since its discovery, aluminium alloys have played a significant role in several sectors of industrial developments. The combination of high strength and low density has made these alloys attractive and played a crucial role in the automotive and aerospace industry. However, newer developments have brought exciting possibilities in high temperature and high-temperature alloy developments in the last few years. One of them is the addition of coherent, ordered precipitates of nanometric sizes. These precipitates also promote hierarchical structures and resistance to microstructure coarsening. It is also increasingly realised that controlled segregation at the precipitate/matrix interface can control and improve room and high-temperature properties. This article focuses on these developments that are expected to open up new possibilities and applications in the automotive and energy sectors.

Keywords Aluminium alloys · $L1_2$-ordered precipitates · Coherent interfaces · Segregation · High-temperature strength

1 Introduction

The research on the physical metallurgy of structural materials in India has been greatly influenced by Dr Srikumar Banerjee through his work that inspired generations of younger scientists and his role in mentoring them. The senior author of this article is particularly benefitted, and it is a pleasure to dedicate this article to his memory.

Since the accidental discovery of the age hardening of Al–Cu alloys at the beginning of the last century, there have been newer developments periodically that kept the interests alive in aluminium alloy. The crucial role it plays in the automotive and aerospace industry is also due to the continuous improvements of these alloys. For example, the last three years witnessed an explosion of papers dealing with newer high-temperature capabilities of aluminium alloys. These developments have often relied on newer architectures utilising ordered precipitates and segregation of alloying elements at the precipitate–matrix interfaces. The review attempts to outline these newer developments in the context of structural applications. The various strengthening precipitates in aluminium alloys highlighted in this review is given in Table 1.

2 Strengthening Due to Ordered Precipitates

Aluminium–Copper (Al–Cu) alloys are among the well-known age-hardening alloys widely used in aircraft and automobiles. The high number density of nanometre-sized metastable phases (θ''/θ' *precipitates*) offer promising strength at temperatures above 150 °C [17]. The solvus of these metastable phases determine the domain available for the alloy design [18]. For age-hardening, the Al–Cu alloys with Cu content 0.5–2.5 at% were first homogenised near eutectic temperature (popularly known as *solution treatment or solutionising*), followed by water quenching, and finally, natural or artificial ageing (150–200 °C). The solution treatment was carried out above the solvus line to allow the solute atom to dissolve into the Al matrix resulting in a single-phase known as the α-Al phase. The

✉ Kamanio Chattopadhyay
kamanio@iisc.ac.in

[1] Department of Materials Engineering, Indian Institute of Science, Bangalore 560012, India

Table 1 Summary of precipitate shape, space group and lattice parameters of various phases formed in Al–Cu, Al–TM (TM = Sc or Zr), Al–Mg–Si, Al–Cu–Mg–Si and Al–Zn–Mg–Cu alloys

Phase	Shape	Space group	Lattice parameters	References
Al–Cu alloys				
θ“	Plate	P4/mmm	$a = b = 4.04$ Å, $c = 7.68$ Å	[1]
θ’	Plate	I4/mmm	$a = b = 4.04$ Å, $c = 5.80$ Å	[2]
θ	Irregular	I4/mcm	$a = b = 6.06$ Å, $c = 4.87$ Å	[2]
Al–TM alloys (TM = Sc or Zr)				
Al_3Sc	Spherical	Pm-3 m	$a = 4.103$ Å	[3]
Al_3Zr	Spherical	Pm-3 m	$a = 4.08$ Å	[4]
Al–Mg–Si alloys				
β”	Needle	C2/m	$a = 15.16$ Å, $b = 4.05$ Å, $c = 6.74$ Å and $\beta = 105.3°$	[5]
β’	Rod	$P6_3/m$	$a = 7.15$ Å, $c = 12.15$ Å, $\gamma = 120°$	[6]
*U*1	Needle	P3m1	$a = b = 4.05$ Å, $c = 6.74$ Å, $\gamma = 120°$	[7]
*U*2	Needle	Pnma	$a = 6.75$ Å, $b = 4.05$ Å, $b = 7.94$ Å	[8]
B’	Lath	P6	$a = b = 10.4$ Å, $c = 4.05$ Å, $\gamma = 120°$	[9]
β	Needle	Fm3m	$a = 6.39$ Å	[6]
Al–Cu–Mg–Si alloys				
L	Needle	–	$a = 8.0$ Å, $c = 7.0$ Å	[10]
S	–	P-6m2	$a = b = 7.0$ Å, $c = 4.05$ Å	[11]
C	Plate	$P2_1/m$	$a = 10.32$ Å, $b = 8.1$ Å, $c = 4.05$ Å, $\gamma = 101°$	[11]
QP	Needle	Hexagonal	$a = b = 3.93$ Å, $c = 4.05$ Å	[12]
QC	Needle	P62m	$a = b = 6.7$ Å, $c = 4.05$ Å	[12]
Q’	Lath	P6	$a = 10.3$ Å, $c = 4.05$ Å, $\gamma = 120°$	[13]
Q	Lath	P6	$a = 10.4$ Å, $c = 4.01$ Å, $\gamma = 120°$	[14]
Al–Zn–Mg–Cu alloys				
η’	Plate	P-6m2	$a = 4.96$ Å and $c = 14.02$ Å	[15]
η	Disc	$P6_3/mmc$	$a = 5.22$ Å and $c = 8.57$ Å	[16]

quenching in water helps to retain the single phase and is termed as the *supersaturated solid solution* (α-Al_{SS}). The solid solution is further decomposed into various metastable phases through heat treatments at various temperatures. These are designated as GP zones, θ“ and θ’. The precipitation sequence is rather complex, depending upon the ageing temperature and the degree of solute supersaturation. The hierarchy of the precipitation sequence in copper-containing alloys is:

$$\alpha - Al_{SS} \rightarrow \text{GP zones} \rightarrow \theta''(Al_3Cu) \rightarrow \theta'(Al_2Cu) \rightarrow \theta\ (Al_2Cu \text{ equilibrium phase})$$

With the recent advancements in the characterisation techniques like high-resolution transmission electron microscopy and atom probe tomography, the precipitate structure can be resolved [18]. The precipitation usually starts with the formation of Guinier–Preston (GP) zones. These are monolayers of Cu atoms on the {100} plane of Al lattice, forming disc-shaped precipitates [19, 20]. θ“ phase forms at higher ageing temperature (130–170 °C). An accepted structural model for θ” that was proposed by Gerold consists of the ordered stacking of Cu layer separated by three Al layers with the stoichiometry Al_3Cu, Fig. 1a [1]. The metastable θ’ phase is the main strengthening phase with stoichiometry Al_2Cu, has a body-centred tetragonal structure with space group I4/mmm and lattice parameters of $a = b = 4.04$ Å and $c = 5.80$ Å [2]. Figure 1b shows the θ’ plate in the α-Al matrix [21]. The plate-like θ’ phase has three variants, and the orientational relationship with respect to Al matrix can be expressed as: $(001)_{\theta'} \| (001)_{Al}$, $[100]_{\theta'} \| [100]_{Al}$; $(010)_{\theta'} \| (010)_{Al}$, $[100]_{\theta'} \| [100]_{Al}$ and $(100)_{\theta'} \| (100)_{Al}$, $[010]_{\theta'} \| [010]_{Al}$ [22]. The θ’ plates exhibit a high aspect ratio with a large anisotropy in the interfacial energy and elastic strain energy between coherent and semi-coherent interfaces [22]. The broad face is coherent with the matrix possessing a smaller interfacial energy value than the semi-coherent interface. The precipitation sequence terminates with the transformation of the θ’ phase to the equilibrium θ phase, having a tetragonal C16 crystal structure and is incoherent with the Al matrix.

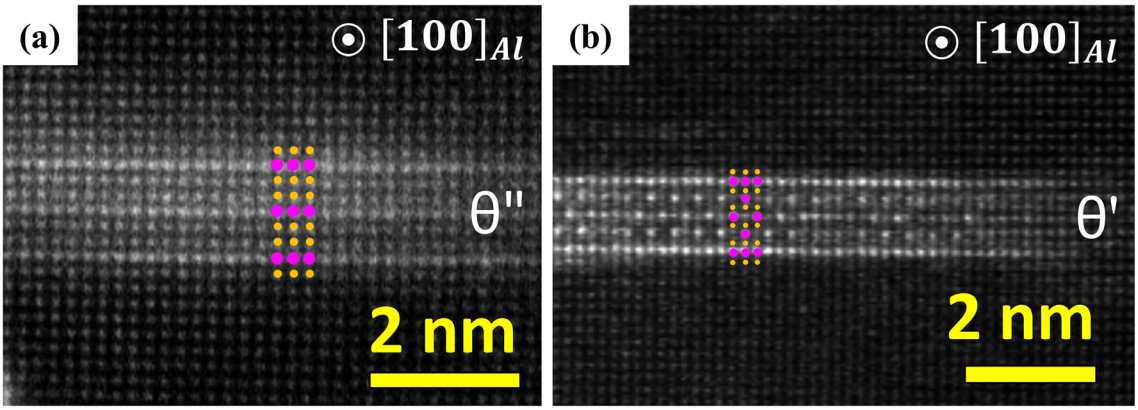

Fig. 1 High-resolution HAADF-STEM micrographs of **a** θ“ plate, and **b** θ’ plate [21]

The addition of transition elements (Sc, Zr, Nb, V, Hf) to aluminium shows potential for forming ordered precipitates in the Al matrix. The high supersaturation of these elements during the casting process (rapid solidification or conventional) results in the decomposition of the supersaturated solution leading to the precipitation of the $L1_2$-ordered phase. Scandium forms a stable Al_3Sc phase. It has a cubic lattice structure of Cu_3Au type with lattice parameter a = 4.10 Å and space group Pm-3 m [3]. All other transition elements result in the metastable $L1_2$-ordered phase. These $L1_2$-ordered precipitates in the dilute aluminium alloys have better thermal stability at elevated temperatures (200–450 °C) than existing commercial 2xxx series Al alloys. However, these dilute Al alloys lack strength at room temperature and elevated temperature. The strengthening effect due to the formation of these coherent precipitates in the α-Al matrix can be quantified based on the precipitate size and the volume fraction. The moving dislocations will shear the particles smaller than a critical radius. At large sizes, the dislocations bow around the precipitate. The shear stress required for a dislocation to loop around the precipitate was first described by Orowan and can be calculated theoretically by equation [23, 24]:

$$\Delta\sigma_{\text{orowan}} = \frac{MGb}{2\pi\sqrt{1-\nu}} \cdot \frac{1}{\lambda} \cdot \ln\frac{\pi d}{4b} \tag{1}$$

$$\lambda = \frac{d}{\sqrt{f} + 0.90f + 2.25(f)^{3/2}} \tag{2}$$

where M is the Taylor factor (3.06) for the FCC Al matrix, G_{Al} is shear modulus ($\sim$ 28 GPa), b is Burgers vector ($\sim$ 0.286 nm), ν is Poisson’s ratio ($\sim$ 0.34) of the α-Al matrix, f is the volume fraction of the precipitates in the α-Al matrix, d is the average particle diameter, and λ is the inter-particle spacing after heat treatment.

For the same precipitate size, a higher volume fraction of precipitates in the α-Al matrix resulted in a higher strength increment, as shown in Fig. 2. However, the limited solubility of transition elements at equilibrium resulted in a lower volume fraction of the strengthening phase ($L1_2$-ordered precipitates) in the α-Al matrix. The maximum solubility of Sc in α-Al is 0.23 at%, and Zr is 0.083 at%, which is much lower than Cu (2.45 at%) and Si (1.65 at%) [4]. Therefore, the strength contribution from the $L1_2$ precipitates is not significant compared to the other strengthening phases formed in the existing commercial alloys. Table 2 compares the 0.2% proof stress reported for dilute Al alloys with existing commercial 2xxx series alloys. The strengthening contributions in 2xxx series alloys were attributed to the shear resistant Cu-rich θ” and θ’ plates in the α-Al matrix formed during ageing between 150 and 200 °C.

The addition of Sc to Al–Cu alloys has attracted wide attention due to the possibility of coexistence of both $L1_2$-ordered Al_3Sc precipitates and θ’-Al_2Cu strengthening

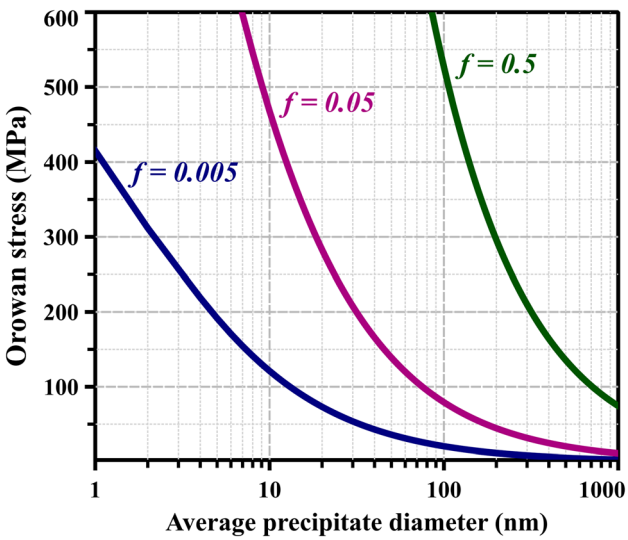

Fig. 2 Orowan stress as a function of average precipitate diameter for the various volume fraction of strengthening $L1_2$ phase [21]

Table 2 Heat treatment route, strengthening phase, and yield strength (0.2% proof stress) of dilute Al alloys, commercial 2219 and 2024 alloys

Alloys (at%)	Heat treatment route		Strengthening phase	Yield strength (MPa)	References
	Solution treatment	Ageing			
Al-0.24Sc	600 °C/72 h	340 °C/20 h	Al_3Sc	147 ± 10	[25]
Al-0.06Zr	460 °C/12 h cold rolled	350 °C/1 h	Al_3Zr	141	[26]
Al-0.24Sc-0.2Zr	600 °C/72 h	340 °C/20 h	Al_3(Sc, Zr)	176 ± 6	[25]
Al-0.02Er	460 °C/12 h cold rolled	350 °C/1 h	Al_3Er	144	[26]
Al-0.06Zr-0.02Er	460 °C/12 h cold rolled	350 °C/1 h	Al_3(Zr, Er)	162	[26]
Al-2Cu	535 °C	190 °C/5 h	θ“/θ’ plates	265 ± 16	[27]
2219-T851	535 °C	190 °C/18 h	θ”/θ’ plates	352 ± 18	[28]
2024-T3	500 °C/1 h	180 °C/10 h	θ“/θ’ plates	350	[29]

phases in the α-Al matrix [30–34]. However, the increase in Sc concentration in Al-2 at% Cu alloy has an adverse effect on the solubility of Cu in the α-Al matrix. In contrast, Cu has a limited effect on Sc solubility. The ageing at higher temperatures (> 260 °C) forms W-phase ($Al_{8-x}Cu_{4+x}Sc$) and is considered detrimental for tensile properties [35, 36]. The Al_3Sc precipitates are formed during ageing between 200 and 400 °C, whereas θ’ plates nucleate below 200 °C.

In the past few years, considerable attention has been given to designing heat treatments to take advantage of Al_3Sc and Al_2Cu (θ’) phases in Al–Cu–Sc alloys with improved thermal stability and high-temperature performance. Segregation of transition elements in the dendritic interiors is generally observed during conventional casting. Alloys are typically held at higher temperatures to achieve homogenisation. Often, the initial ageing was conducted directly on as-cast Al–Sc–Cu-based alloys to form $L1_2$-ordered Al_3Sc precipitates in the α-Al matrix. The formation of Al_3Sc precipitates in the α-Al matrix further helps in the nucleation of θ”/θ’ plates [34]. The orientation relationship between Al_3Sc precipitates and θ’ plates was found to be $(001)_{\theta'} \| \{001\}Al_3Sc$, $[100]_{\theta'} \| < 100 > Al_3Sc$, whereas the orientation relationship between θ’ plates and Al matrix remained unchanged. Chen et al. showed the heterogeneous precipitation of θ’ plates at the {100} plane of Al_3Sc precipitates and the formation of an enclosed group [32]. The existence of $L1_2$-ordered precipitates suppresses the homogeneous nucleation of θ’ plates and promotes heterogeneous nucleation, leading to enhanced number density and higher volume fraction of θ’ plates. Further, the growth rate of heterogeneously nucleated θ’ plates was reported to be two times lower than homogeneously nucleated plates [32]. The precipitation kinetics of θ“ and θ’ plates were enhanced in Sc-containing Al–Cu alloys compared to the binary alloys [37, 38]. Yang et al. reported ∼ 40% reduction in θ’ plate length and ∼ 80% increment in the number density of θ’ plates after 0.18 at% Sc addition to Al-1.08 at% Cu alloy and aged at 250 °C for 8 h [37]. Few reports emphasised a two-step ageing process in Al–Cu–Sc based alloys modified with Zr, V, and Ti. It results in forming coarsening resistant Al_3Sc precipitates by allowing the segregation of low diffusing transition elements (Zr, V or Ti) at the Al_3Sc precipitate/matrix interface during ageing at higher temperatures [39–41]. The addition of Zr to Al–Cu–Sc alloys was reported to enhance the high-temperature performance of the alloys [42–45]. Dorin et al. systematically studied the addition of Sc and Zr to Al-2 at% Cu alloy [44]. They demonstrated that adding 0.06 at % Sc or 0.03 at% Zr to Al–Cu alloys improves room temperature yield strength by ∼ 50 MPa after ageing at 160 °C for 10 h compared to the binary alloy. The combined addition of Sc and Zr results in ∼ 150 MPa increment in the yield strength due to the refinement of θ’ plates attributing to the presence of thermally stable core–shell Al_3(Sc, Zr) precipitates in the α-Al matrix [43, 44].

Mondol et al. attempted to modify 2219 commercial alloys by alloying with 0.8 wt% Sc and 0.45 wt% Mg. They reported the precipitation of Al_3Sc and Al_3(Sc, Zr) core–shell precipitates in the Al matrix during suction casting using water-chilled copper mould [46]. The ordered precipitates with less than 14 nm diameter were Al_3Sc type, and those above 15 nm had Al_3(Sc, Zr)-type stoichiometry. Figure 3a shows the TEM EDS analysis of core–shell Al_3(Sc, Zr) precipitate formed in the Al matrix. The 3D-APT map of $L1_2$-order precipitates is shown in Fig. 3b. The formation of fine, coherent $L1_2$-ordered precipitates improves yield strength by 37% without harming ductility. The microhardness curve depicts the modified 2219ScMg alloy stable at 200 °C for 1000 h. Later, the authors documented 32% and 42% improvement in yield strength of commercial 2219 alloys at room temperature and 250 °C, respectively, with the combined addition of

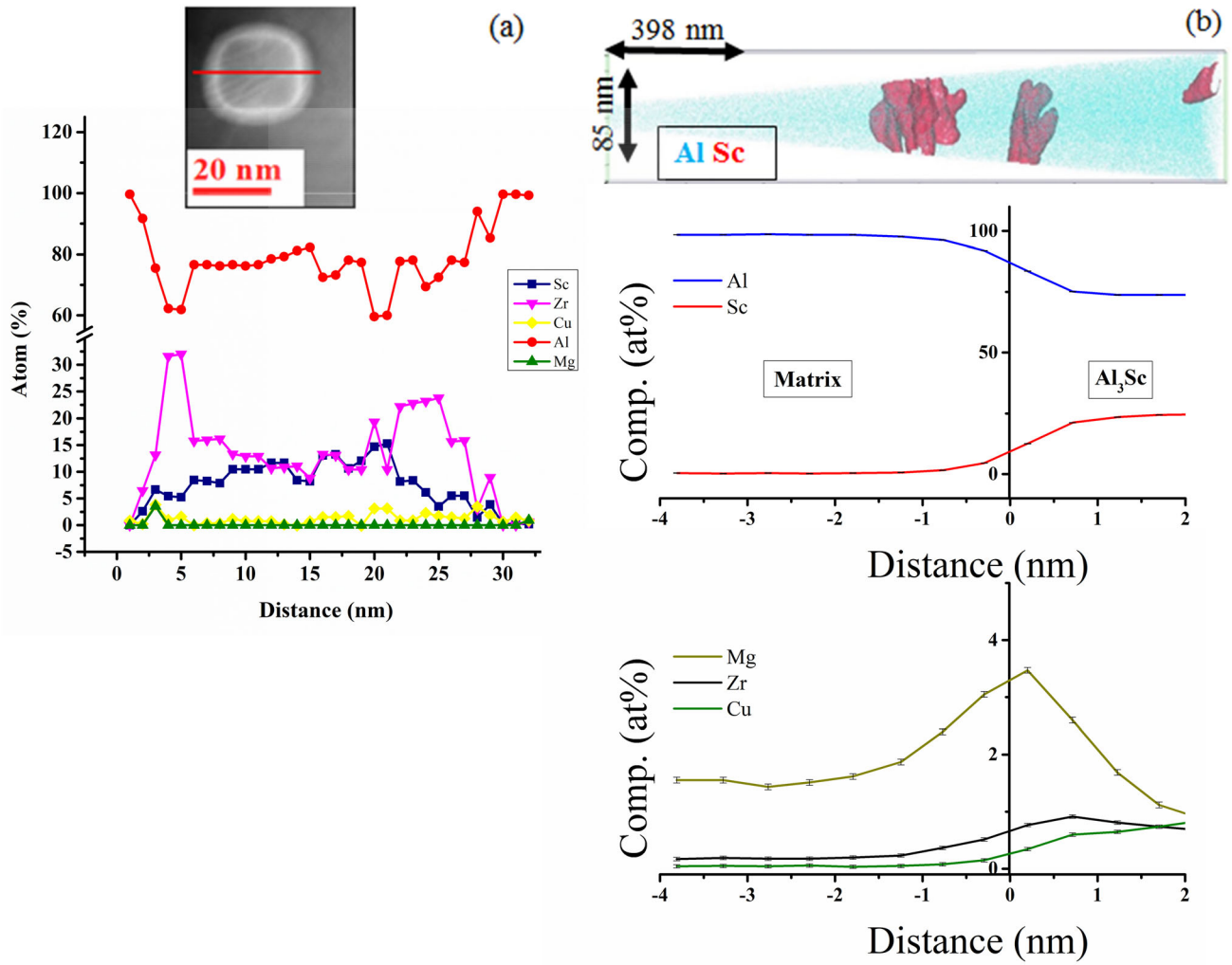

Fig. 3 2219ScMg alloys. **a** EDS analysis of core–shell $Al_3(Sc, Zr)$ precipitates formed in Al matrix during suction casting. Inset shows the core–shell precipitate, **b** 3D-APT reconstruction map with Sc-0.55% iso-concentration surface, **c** and **d** Proxigram of Al, Sc, Mg, Zr and Cu across the interface [46]

0.15 at% Sc and 0.15 at% Zr [47]. Figure 4a, b displays the formation of plate precipitates along with $Al_3(Sc, Zr)$ spherical precipitates in the Al matrix in Sc-, Zr-modified 2219 commercial alloys. The high-resolution HAADF-STEM image in Fig. 4c, d indicates that the $Al_3(Sc, Zr)$ precipitates are coherent with the matrix, and both θ" and θ' plates are nucleated on ordered precipitates. Further, the interfacial segregation of Zr along with Sc aids in stabilising θ' plates against coarsening at elevated temperatures (300 °C) [45]. The presence of low diffusing elements like Sc or Zr (D_{Sc} = 19.0 × 10^{-20} and D_{Zr} = 1.14 × 10^{-20} m^2/s^{-1} at 300 °C in the α-Al matrix) at the interface of plates acts as a kinetic barrier due to Zener-drag effect. Thus, the addition of transition elements is thermodynamically and kinetically favourable to increase the coarsening resistance of θ' plates and enhance the high-temperature performance of the alloys.

The minor addition of Nb (∼ 0.10 at%) promotes continuous precipitation of the Al_3Zr phase [27]. The formation of $L1_2$-ordered Al_3Zr precipitates improves the yield strength of Al–Cu–Nb–Zr alloy compared to the binary Al–Cu alloy [27]. After three-step heat treatment, the reported room temperature yield strength was 460 ± 18 MPa for Al–Cu–Nb–Zr alloy. However, around ∼ 50% drop in ductility was observed. The composite microstructure, as shown in Fig. 5a–c, enhances the high-temperature (250 °C) yield strength of the alloy (250 ± 16 MPa at 250 °C) due to the slower growth kinetics of the θ' plates.

Mondol et al. extended this approach to commercial 2219 alloys. They reported ∼ 57 MPa and ∼ 35 MPa enhancement in yield strength at room temperature and 200 °C, respectively, with the addition of Zr and Nb [28]. The microstructure of peak-aged 2219NbZr alloy is shown

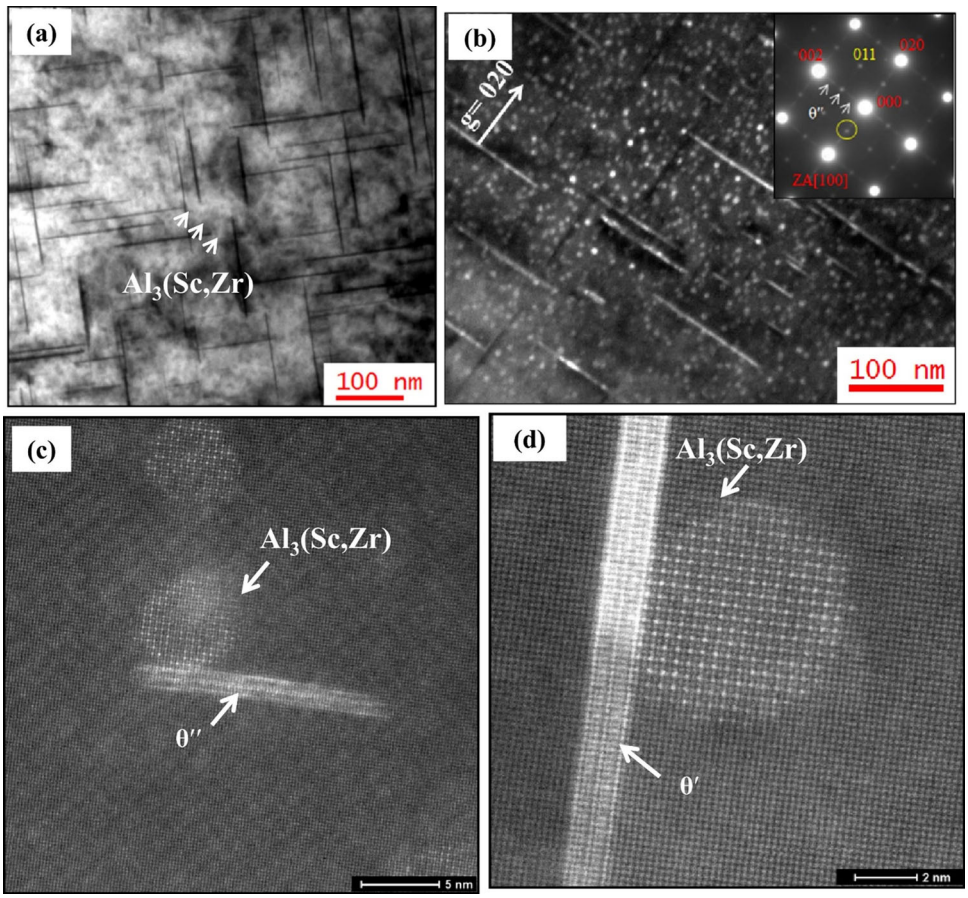

Fig. 4 2219ScZr alloys. **a** Bright-field **b** Dark-field TEM image showing the θ' plates and Al_3(Sc,Zr) precipitates formed in the Al matrix after ageing at 200 °C-10 h. The prior ageing treatment was 375 °C-40 h and 535 °C-30 min. High-resolution HAADF-STEM image along $[001]_{Al}$ zone axis showing heterogeneous nucleation of **c** θ" plates, and **d** θ' plate on pre-existing Al_3(Sc, Zr) precipitates [47]

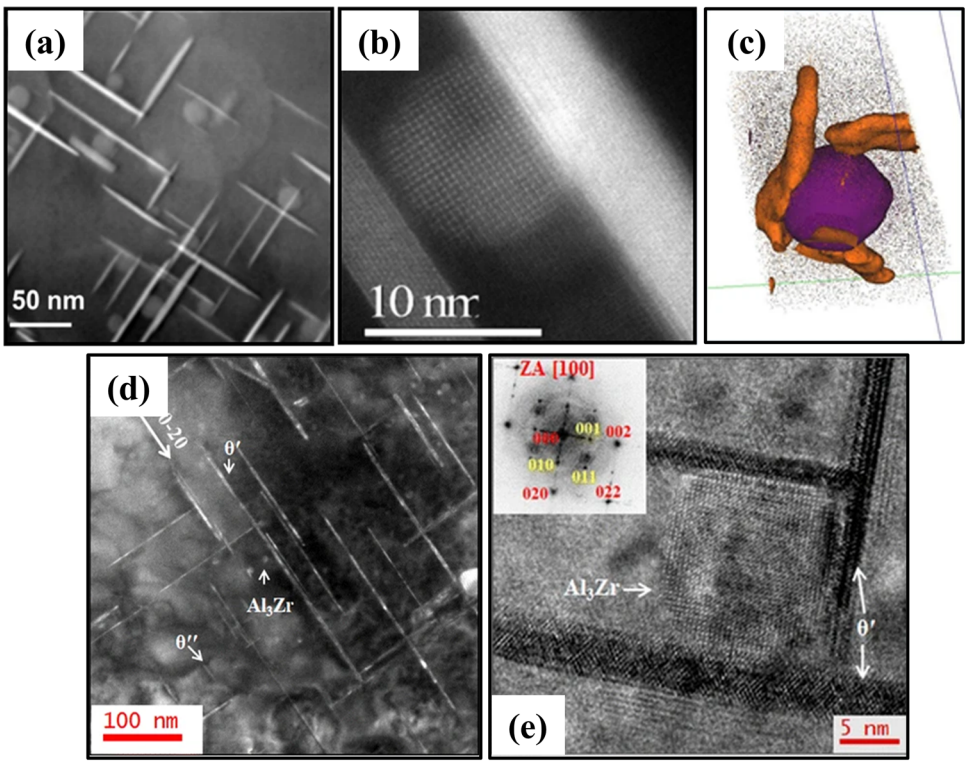

Fig. 5 **a**, **d** HAADF-STEM image, and **b, e** high-resolution micrograph along [001] zone axis showing heterogeneous nucleation of plate precipitates on pre-existing spherical Al_3Zr precipitate in Al–Cu–Nb–Zr alloys after ageing at 190 °C for 5 h [27] and in 2219NbZr after ageing at 200 °C for 10 h [28], respectively. **c** 3D-APT reconstruction map showing heterogeneous nucleation of the plates on spherical Al_3Zr precipitate in Al–Cu–Nb–Zr alloy [27]

in Fig. 5d–e, evidencing the heterogeneous nucleation of θ" and θ' plates on pre-existing Al_3Zr precipitates. An increment of $\sim$ 56 MPa in room temperature yield strength was recently reported by adding 0.08 at% of Zr to Al-1.3 at% Cu alloy and following a complex heat treatment route [48]. Further, the combined addition of 0.04 at% Er and 0.08 at% Zr resulted in $\sim$ 88 MPa of strength increment.

Another class of heat-treatable Al alloys is 6xxx series alloys (Al–Mg–Si), which are used in the cast, wrought, and extruded forms. These alloys are attractive for automotive and aircraft industries due to their excellent corrosion resistance, weldability and superior surface properties. The strength of these alloys can significantly be enhanced through precipitation of a high number density of nanometer-sized metastable phases during artificial ageing. The precipitation sequence in such alloys is:

$$\text{SSSS} \rightarrow \text{atomic clusters (Mg or Si)} \rightarrow \text{GPZ} \rightarrow \beta'' \rightarrow \beta', U1\ U2,\ B' \rightarrow \beta\ (\text{stable, } Mg_2Si, \text{ plate-shaped}), \text{Si}.$$

β" is a fine needle-shaped metastable Mg_5Si_6 phase, aligned along [100] direction of Al matrix [5]. The proposed crystal structure for β" is monoclinic (space group: C2/m) with a = 15.16 Å, b = 4.05 Å, c = 6.74 Å and β = 105.3°. β' precipitates formed in precipitation sequence after β". They are rod-shaped Mg_9Si_5 phase, aligned along [100] direction of Al matrix, with the hexagonal crystal structure (space group: $P6_3/m$) and lattice parameters: a = 7.15 Å, c = 12.15 Å, γ = 120° [6]. The $U1$, $U2$ and B' phases are also known as Type-A, Type-B and Type-C, respectively, and mostly appear on over-ageing [7–9]. The $U1$ and $U2$ are needle-shaped and B' is lath shaped. $U1$ or Type-A are trigonal crystal structure (space group: P3ml) with lattice parameters: $a = b$ = 4.05 Å, c = 6.74 Å, γ = 120°, $U2$ or Type-B are orthorhombic (space group: Pnma) with lattice parameters: a = 6.75 Å, b = 4.05 Å, b = 7.94 Å and B' is hexagonal (space group: P6) with lattice parameters: $a = b$ = 10.4 Å, c = 4.05 Å, γ = 120°. The equilibrium β-Mg_2Si phase is a stable phase having a cubic crystal structure (space group: Fm3m) with a = 6.39 Å [6]. The equilibrium β-Mg_2Si phase does not significantly strengthen the Al matrix compared to the intermediate metastable phases.

The strength of 6xxx alloys directly depends on the metastable precipitates. Therefore, many attempts have been made to improve the precipitation kinetics by heat treatment and/or alloying additions. The pre-ageing of AA6111 alloy is an effective way to modify the mechanical properties of the alloys by avoiding the determinantal effects of natural ageing [49]. Pre-ageing also enhances the artificial ageing kinetics during the early ageing period [50]. Another method to modify the precipitation sequence is by interrupting quenching [51]. The Al–Mg–Si alloy was treated at 570 °C, and then quenched in a pre-heated bath at a temperature range of 150–250 °C, followed by water quenching at room temperature. The alloys were then artificial aged at 170 °C. The authors reported the enhanced precipitation of the β" metastable phase due to increased quenched-in vacancies. Though the heat treatment modifications like pre-ageing, intermediate quenching, etc., suppress the determinantal effects of natural ageing, the alloying addition with Ge [52, 53], Cu [10, 11, 54, 55], Cd [56], Ag [57–59], Zn [60], Li [52], Sc and Zr has recently attracted attention due to the accelerated ageing response and significant improvement in strength. The enhanced ageing response is related to the modification in the precipitation sequence by the alloying additions. Due to similar electronic properties, Ge was reported to replace Si atoms in the β" phase [53], while Li was reported to substitute Mg sites in the β" structure [52]. Cd forms Cd-rich precipitates in the early stage of artificial ageing and acts as nucleation sites for needle-shaped β" precipitates that lead to the observed Q'/C type triangular sub-units in the matrix [56]. HAADF-STEM further reveals that Cd-atoms incorporated into β" precipitates leads to a disordered structure. The addition of Ag to high Al–Cu–Mg alloys with a high Cu/Mg ratio results in the formation of a thermally stable coherent Ω phase along $\{111\}_{Al}$ habit plane [61]. Ag has also been found to segregate at precipitate/matrix interface [58, 59, 62]. However, the addition of Cu results in the suppression of the β" phase and promotes several new metastable phases. The precipitation sequence in Al–Cu–Mg–Si as reported in the literature is [10, 12, 59]:

$$\text{SSSS} \rightarrow \text{Atomic clusters} \rightarrow \text{GPZ} \rightarrow \beta'',\ L/S/C,\ QP,\ QC \rightarrow \beta',\ Q' \rightarrow Q, \text{Si}$$

Recently, Sunde et al. studied the effect of Cu on various intermediate precipitates in Al–Mg–Si alloys. A detailed study was presented on the correlation between microstructure and mechanical strength [63]. The authors reported that the high Cu content alloy shows higher yield strength (0.2% proof stress: 406 MPa) due to the presence of fine and dense lath-type L precipitates along with few intermediate metastable phases like β", β' and Q'. Further, these precipitates have been found to coarsen slowly in high Cu-containing alloys. High Cu and high Mg content promote enhanced precipitation and hardening ability, making them suitable for automotive body panel applications. Atom probe tomography measurements and first-principal calculations demonstrate that the presence of interstitial Cu atoms stabilises the B' variant formed in Cu-

containing Al–Mg–Si alloys for longer ageing time compared to β' phase formed in Cu-free Al–Mg–Si alloys.

Unlike Al–Cu alloys, the effect of transition elements like Sc or Zr has not been much explored in 6xxx series alloys. Within the limited reports, the Sc additions to Al–Mg–Si alloys show both positive and negative effects on the mechanical properties of the base alloy [64–66]. The addition of Sc and Si reduces the room temperature solubility of both elements resulting in the formation of the $AlSc_2Si_2$ phase. The strong interaction of Sc with Si negatively affects strength, which could be rectified by designing a suitable heat treatment or thermo-mechanical processing route. On the other hand, trace additions of Si with Sc have been found to improve the precipitation kinetics of the Al_3Sc phase, where Si has been found to substitute Al. The addition of Sc to commercial 6061 alloys have resulted in a slow hardening response and lowered overall strength [65]. However, the hardness gets stabilised at a longer ageing time, attributed to $L1_2$-Al_3Sc-ordered nanoprecipitates. The Sc addition to Al–Mg–Si alloy, on ageing at 180 °C, leads to the formation of disordered β'' precipitates. These disordered precipitates evolve to β'/B'/$U2$ sub-units that further lead to the formation of β''/β'/B'/$U2$ composite precipitates during over-ageing that improves thermal stability of the Sc-added Al–Mg–Si alloys.

However, the addition of Zr and Sc seems to be an effective way to enhance the strength of the base alloy by adequate precipitation of ordered precipitates ($L1_2$-Al_3(Sc, Zr)) with modifications in the heat treatment route and processing conditions. Few reports suggest a slower ageing response with these additions. However, the thermal stability of microstructure due to the presence of ordered precipitates cannot be neglected [64, 66]. For instance, the addition of Sc and Zr to 6061 alloy shows a slower ageing response at 190 °C, resulting in lower yield strength of 321 MPa (aged for 5 h) than base 6061 alloys (350 MPa) [64]. On prolonged ageing (36 h), a significant drop ($\sim$ 19%) in the yield strength of 6061 alloys was reported compared to only a $\sim$ 6% drop in ScZr-modified 6061 alloys. Rokhlin et al. observed a positive effect of Sc and Zr addition to Al–Mg–Si alloys and reported an increase in the strength without compromising ductility [67]. Designing an appropriate heat treatment is required to take advantage of Sc- and Zr-based ordered precipitates. Dobrzynska et al. studied the effect of casting parameters (solidification rates) on the processing of the Al-1%Mg-0.6%Si (wt%) with Sc/Zr [68]. Rapid solidification during melt spinning results in high supersaturation of Sc and Zr. On annealing between 400 and 540 °C, the spherical and coherent Al_3Zr or Al_3(Sc, Zr) precipitates have been reported. The chilled copper mould cast alloys show a significant refinement in grain size due to the formation of primary Al_3(Sc, Zr) particles in the matrix. These alloys were subjected to a non-standard heat treatment schedule by introducing an additional annealing step at 300–350 °C [69]. The pre-annealing results in the formation of Al_3(Sc, Zr) precipitates in the matrix, which grows during annealing at 540 °C. This step results in the complete dissolution of Mg_2Si particles into the Al matrix. Final ageing at 165 °C leads to needle-shaped Q' phases that coexist with Al_3(Sc, Zr)-ordered precipitates. A similar heat treatment route was applied to Al–Cu–Mg–Si alloys modified with Sc and/or Zr. Discontinuous precipitation of the $L1_2$-ordered Al_3Sc phase with coexisting continuous precipitation could be observed in Sc-containing Al–Cu–Mg–Si alloys. The Al_3Sc precipitates coarsen rapidly during annealing at 540 °C, resulting in the coherency loss. The addition of Zr promotes the continuous precipitation of the Al_3Sc phase. However, it also slows down the growth of ordered precipitates. In the Zr-modified Al–Mg–Si alloys, instead of water quenching from 535 °C, quenching to 100 °C before water quenching proves to be an effective way to enhance the strengthening effect by promoting β'' phase in the microstructure [70]. Babaniaris et al. further modified the heat treatment route and reported a 60 MPa increase in yield strength in Sc–Zr-modified Al–Mg–Si alloys over the base alloys [71]. The heat treatment route adopted was solution treatment at 575 °C for 5 h followed by water quenching, subsequently aged at 300 °C for 3 h followed by ageing at 450 °C for 3 h and finally aged for a short period at 500 °C. The complex heat treatment route results in the formation of Al_3(Sc, Zr) core–shell precipitates in the matrix, which at later stages provides nucleation sites for MgSi precipitates.

The other important class of heat-treatable alloys is 7xxx series AlZnMgCu-based alloys. These alloys are critical for aerospace and transportation industries due to their high strength among commercial Al alloys [72]. The strengthening, in this case, occurs from the fine dispersion of the $MgZn_2$ phase during artificial ageing [73, 74]. The precipitation sequence in the 7xxx series is:

$$\begin{aligned} \text{SSSS} \rightarrow \text{GPZ} \rightarrow \eta' \ (\text{metastable phase, } MgZn_2) \\ \rightarrow \eta \ (\text{equilibrium phase, } MgZn_2) \end{aligned}$$

This class of alloys after solution heat treatment decomposes to yield two kinds of G.P.Zones; the GPZ-I and GPZ-II, where GPZ-I are Mg-rich clusters on the {100} Al plane and GPZ-II are Zn-rich clusters on {111} Al plane [16, 75, 76]. Sha et al. observed the appearance of GPZ-I during the early stages of precipitation (< 30 min of ageing at 121 °C) with Zn/Mg ratio $\sim$ 0.9 in 7050 alloys [75]. Buha et al. observed the formation of GPZ-II in 7050 alloys [76]. The appearance of GPZ-II depends on the vacancy supersaturation and is more stable than GPZ-I. It exhibits a plate-like morphology and can transform to η'

phase. The metastable η' phase is $MgZn_2$, space group P-6m2, with lattice parameters: $a = 4.96$ Å and $c = 14.02$ Å [15]. The equilibrium η phase appears on over-ageing having space group $P6_3/mmc$ with lattice parameters: $a = 5.22$ Å and $c = 8.57$ Å [16].

Conventionally, the optimisation of the Zn/Mg ratio can significantly improve the strength of the alloys. Liu et al. reported that the Zn/Mg ratio increases the number density and volume fraction of metastable nanoprecipitates [77]. High Zn content can remarkably improve the strength of the alloys and gives excellent wear properties [78]. However, high Zn content produces unavoidable casting defects such as macro-segregation, cracking and grain coarsening. Therefore, the Zn concentration in traditional commercial alloys is limited to 10 wt%. Meng et al. reported a rapidly solidified alloy with Zn content close to 27 wt% using melt spinning and extrusion [79]. The alloy, however, shows poor ductility of ∼ 2.8% with a medium yield strength of 466 MPa. The Zn particles, which remained undissolved in the matrix, promote defects that harm the ductility of alloys. Recently, the same group reported an increase in the yield strength to 678.8 MPa with appreciable ductility (9.1%) by reducing the Zn content down to 13.2 wt% along with a small amount of Zr (0.2 wt%) [80]. The high strength of the alloys was due to the precipitation of the high-density η' phase during ageing. Won et al. reported a significant improvement in the tensile properties by optimising Mg and Cu concentration [81]. Compared to 7056 alloys, a 21% increase in yield strength (though at the cost of ductility) was reported with an increase in Mg and Cu concentration from 1.8 to 3 wt% [16]. The increase in solute concentration results in the nanoscopic structural distortions leading to high strength.

Microalloying with Ti [82], V [83], Sc [84], Zr [85–88] or Sc + Zr [89–97] shows great potential in developing high strength 7xxx series alloys. High supersaturation of Sc or Zr results in the formation of Al_3Sc or Al_3Zr or Al_3(Sc, Zr) metastable coherent precipitates, which imparts additional strength to the alloys. These dispersoids pin dislocations and inhibit the dynamic recrystallisation and recovery during hot deformation or extrusion [85, 87]. Shi et al. reported an increase in activation energy for hot deformation from 229.4 to 255.2 kJ/mol with the addition of 0.19 wt% Zr to 7150 alloy due to inhibition of dislocation motion by Al_3Zr dispersoids [85]. Adding V (∼ 0.11–0.19 wt%) to 7150 alloys inhibits dynamic recrystallisation by forming $Al_{21}V_2$ dispersoids [83]. However, the maximum increase in the activation energy for hot deformation was observed with low V content (∼ 0.03–0.05 wt%), where vanadium solute diffusion was considered the deformation rate-controlling step. Sc addition to Al–Zn–Mg–Cu alloy results in the optimum combination of yield strength (∼ 373.3 Mpa) and elongation (∼ 10.6%) after extrusion at 350 °C due to the formation of Al_3Sc dispersoids in the matrix [84]. The formation of nanometer-sized Al_3Sc precipitates contributes 144 Mpa to the total strength. The chemical driving force to obtain the desired volume fraction of these fine coherent dispersoids in the matrix depends upon the supersaturation of these elements. The supersaturation can be obtained by direct chill casting techniques.

Further, optimisation of heat treatment is required to control the kinetics and the growth of these precipitates, which directly impacts the tensile properties of the alloys. Guo et al. observed an additional homogenisation step at 300 °C that significantly increases the recrystallisation resistance in 7150 alloys modified with Zr. The dispersion of Al_3Zr in the Al matrix has led to the reduction in the precipitate free zone. This prevents partial anodic reaction by decreasing the electrochemical differences between grain and grain boundaries, improving the resistance against stress corrosion cracking, intergranular corrosion, and exfoliation corrosion [92]. Recent research shows that the combined addition of Sc and Zr results in better mechanical properties than base alloys. Senkov et al. reported an increase in yield strength by 75–118 MPa, 15–22% of total yield strength with 0.114 at% Sc and 0.056 at% Zr additions to Al–Zn–Mg–Cu alloys after solutionising at 460–480 °C [90]. A maximum volume fraction of $\sim 46 \times 10^{-4}$ of Al_3(Sc, Zr) precipitates after solutionising at 480 °C for 48 h is reported for this case. Zhang et al. showed the best combination of strength (YS:747 MPa, UTS:721 MPa) and ductility (10.9%) by the addition of Sc and Zr and optimising the heat treatment route [89] (solutionising at 470 °C and ageing at 120 °C for 15 h). The peak-aged microstructure contains a high number density of coherent, finely distributed Al_3(Sc, Zr) precipitates in the matrix along with GP zones and η' phase. The increase in Sc/Zr ratio from 1 to 2.5 increases the yield strength by 30 MPa due to the increase in the number density of Al_3(Sc, Zr) dispersoids in the matrix [92].

The comparison of strength and ductility of different series of alloys with microalloying is shown in Fig. 6.

3 Strengthening Due to Elemental Segregation at the Interface of Main Strengthening Phases

The stability of microstructure at elevated temperatures is an essential requirement for precipitation strengthened aluminium alloys. The discussions in previous sections included the influence of $L1_2$-ordered precipitates on the strength and stability of the recently developed Al alloys. These ordered precipitates are stable at the temperature of our interest (200–300 °C). However, the main

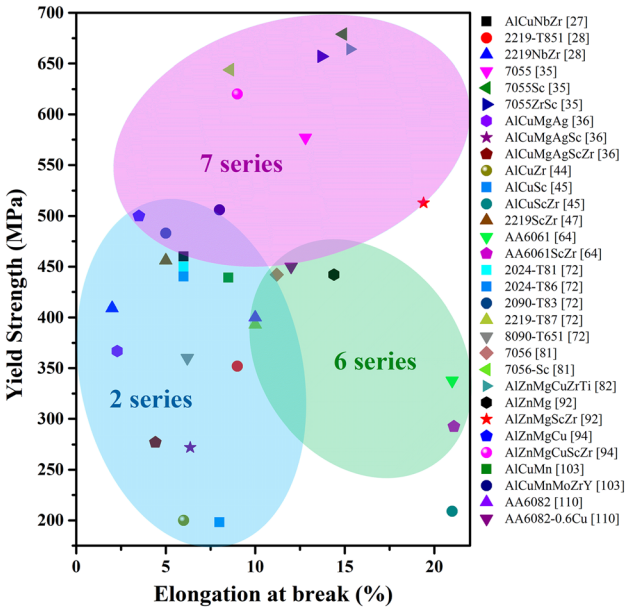

Fig. 6 Room temperature strength ductility map showing new-generation aluminium alloys with existing commercial alloys

strengthening phases in most of these alloys coarsen rapidly above 200 °C [28, 46, 98–101]. In Al–Cu alloys, coarsening of strengthening θ' plates occurs at elevated temperatures (> 200 °C) during later stages of precipitation. At the onset of the coarsening, the thermodynamic driving force for the precipitate growth is negligible. The growth of larger precipitates occurs at the expense of smaller ones due to the establishment of a capillary-driven driving force that emerges due to size differences between the smaller particles and larger particles. The coarsening rate depends upon the diffusion coefficient of solutes in the α-Al matrix (D) and the interfacial energy of the plate–matrix interface (γ). The segregation of solute atoms at the θ' plate/matrix interfaces affects the interfacial energy and plays an important role in controlling the coarsening rate of plates. Therefore, this section is dedicated to the effect of elemental segregation on coarsening behaviour of main strengthening phases and its effect on mechanical properties.

The effect of transition elements (Sc, Ti, Zr, etc.) on the precipitation behaviour and coarsening kinetics of θ' plates in Al–Cu-based alloys have been extensively studied in the past two decades [27, 28, 31, 32, 38, 43, 100, 102, 103]. The Sc addition to Al alloys results in stable $L1_2$-ordered Al_3Sc precipitates in the α-Al matrix [26–31] and this results in the segregation at the plate–matrix interface. The segregation of Sc atoms at the θ' plate/matrix interfaces improves resistance against coarsening and concomitantly improves the mechanical properties of the alloys [38, 104, 105]. Gao et al. observed the Sc segregation around ∼ 2.35 at% at the α-Al/θ' plate interface during ageing at 250 °C [101]. The coarsening resistance was thermodynamically favourable due to the reduction in interfacial energies by the Sc interfacial segregations. The reported reduction in energy due to the interfacial segregation was − 3.76 mJ/m^{-2} at the coherent interface of θ' plates [42]. Further, the increment in the yield strength was ∼ 30 to ∼ 120 MPa with the increase in Sc concentration from 0.06 to 0.18 at% in Al-1.08 at% Cu alloys [38]. However, the Sc microalloying to Al–Cu alloys has been found to reduce the ductility of the Al–Cu alloys. Around ∼ 17% of the decrease in ductility of Al–1.08 at% Cu alloy was observed after adding 0.18 at% Sc to binary alloy. Gao et al. also observed the reduction in creep rates by order of magnitude in Sc-containing Al–Cu alloys [31]. Chen et al. observed that the θ' plates in Al–Cu–Sc alloys are more stable [32]. The stability of the plates is related to the interfacial Sc segregation resulting in a ∼ 25% decrease in the interfacial energy. It results in 2.5 times increase in strength over that obtained in Sc-free alloys. The Cu concentration in the matrix controls the Sc segregation at θ' plate/matrix interface [38]. The Al-2.5Cu-0.3Sc (wt%) alloy had a higher Sc concentration at the interface and better room temperature yield strength (∼ 1.8 times higher) than Al-1.0Cu-0.3Sc and Al-1.5Cu-0.3Sc alloys. The segregation of Sc and Mg at the θ' plate/matrix interface in 2219ScMg alloy stabilises the microstructure up to 1000 h at 200 °C with a yield strength of 495 MPa at room temperature. It is around 34% higher than that obtained in commercial 2219 alloys under similar heat treatment conditions [46]. Rouxel et al. reported the segregation of Zr along with Sc at the θ' plate/matrix interfaces in Al–Cu–Sc–Zr alloys [43]. Slower diffusion of Zr in the α-Al matrix aids in stabilising the θ' plates for more extended periods. The addition of Mn with Sc and Zr effectively stabilises the strengthening precipitates against coarsening up to 300 °C in Al–Cu–Mn–Zr and Al–Cu–Mn–Sc–Zr alloys [42, 100, 102]. Jiang et al. reported the reduction in interfacial energy by ∼ 3.7 mJ/m^2 and ∼ 3.5 mJ/m^2 due to Sc and Zr segregations, respectively, at the coherent interfaces of θ' plates in Al–Cu–Mn–Sc–Zr alloys aged at 190 °C for 18 h and then exposed to 280 °C for 24 h [42]. In the same report, the Mn interfacial segregation at both semi-coherent and coherent interfaces was shown to reduce the interfacial energy by ∼ 73 mJ/m^2 and ∼ 26 mJ/m^2, respectively. Further, the interfacial segregations of Mn, Sc and Zr atoms were shown to reduce the interfacial energies and provide a kinetic diffusion barrier that diminishes the coarsening rate of θ' plates [42]. Recently, Bahl et al. reported a negligible coarsening rate of θ' precipitates in Al–Cu–Mn–Zr alloys at 300 °C exposed for 5000 h. The authors attributed it to Mn and Zr segregation at the θ'/α-Al interfaces [100]. 3D-APT map of AlCuMnZr alloy indicates segregation of Mn and Zr at the

plate/matrix interface. The stability of hardness values after long exposures was primarily due to Orowan strengthening and stress-free transformation strains (SFTS). Ti addition to Al–Cu–Mn–Zr alloys was reported to stabilise θ' precipitates beyond 300 °C [106]. The APT and STEM results revealed that Mn stabilises θ' plates and promotes Zr/Ti segregating at the interface, which eventually leads to a θ'/$L1_2$-Al_3(Zr,Ti)-type stoichiometry. The co-precipitate structure was reportedly stable at 350 °C due to decreased interfacial energy related to the formation of the $L1_2$ structure at the θ' plate interface. Figure 7 displays the schematic of the microstructure evolution with the addition of Sc, Zr, Mn and different heat treatment routes. The $L1_2$-ordered Al_3Sc precipitates can result in high yield strength that can be further enhanced by reducing the coarsening with the help of Zr addition. Zr forms a shell around Al_3Sc precipitates and enhances strength. Further, by providing nucleation sites for plate precipitates (θ"/θ'), an enhanced number density with finer size distribution results that further improves the yield strength. The segregation of Mn and Zr at the plate/matrix interface delays the coarsening of θ' plates by reducing the interfacial energy, resulting in high yield strength compared to base Al–Cu alloys. Thus, the alloying addition with careful selection of heat treatment route may result in newer-generation aluminium alloys to meet the current challenges of aerospace and automobile industries.

The addition of Cu to 6000 series alloy resulted in a different type of precipitates, as discussed in the previous section. Matsuda et al. observed the segregation of Cu at the Q'/α-Al matrix interface with the help of energy-filtered TEM [107]. Later, Weng et al. also showed the Cu segregation using HAADF-STEM at the β' and QP2 precipitate interface [108]. The segregation of Cu accommodates the lattice misfit between β' and Al matrix. Further, the Cu atoms were arranged periodically at the coherent interface of lath-like β' precipitate due to the strong interaction between Cu and Si atoms [109]. The alloys were found to have better thermal stability than Al–Mg–Si alloys at 250 °C [110]. A similar effect was reported with

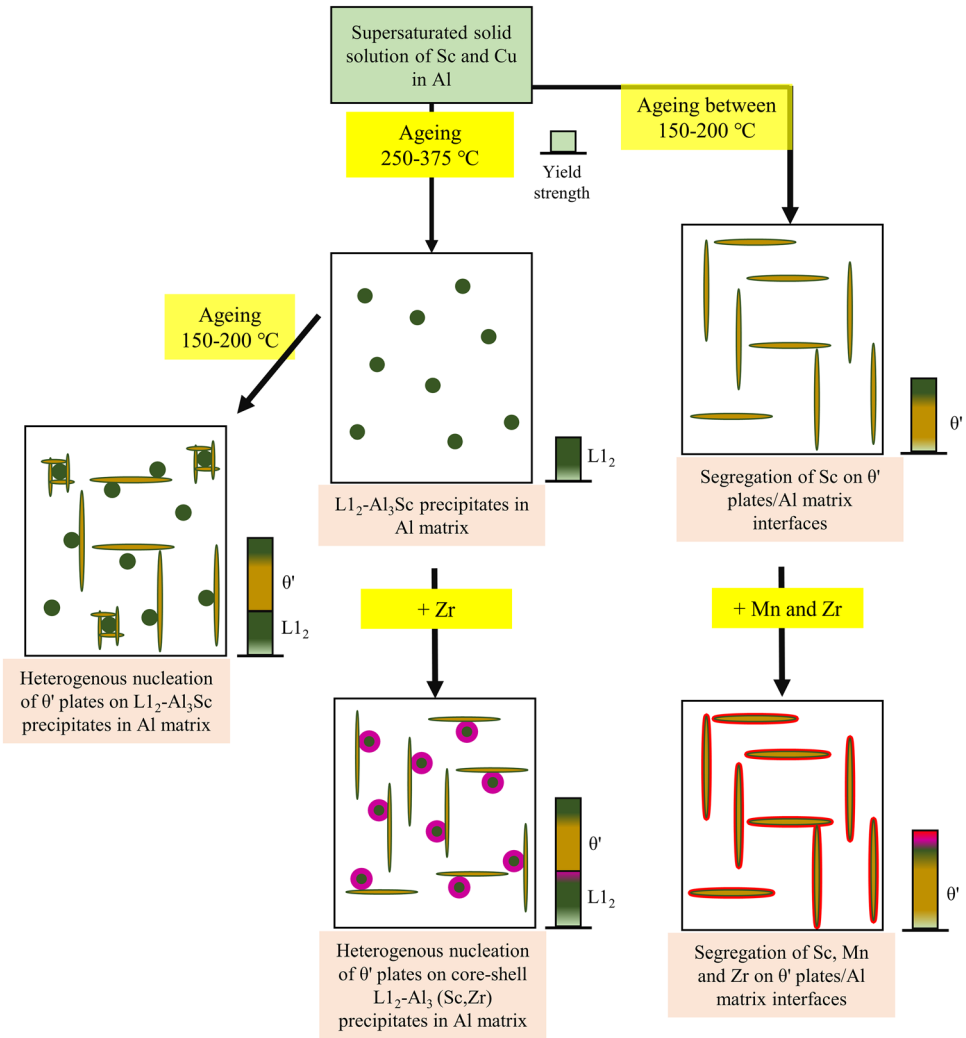

Fig. 7 Schematic of microstructure evolution in Al–Cu alloys after alloying with transition elements like Sc, Zr or Mn and various heat treatments showing an increment in yield strength by precipitating $L1_2$-ordered precipitates in Al matrix or by interfacial segregation at the plate/matrix interface or by both

Ag addition [62, 111]. At initial stages of ageing to Al–Mg–Si–Ag alloys, Ag was reported to segregate at GPZ/α-Al matrix and β"/α-Al matrix interface, which on later stages of ageing were incorporated into the precipitates resulting in QP lattice with disordered structures. Further, the addition of Ag to Al–Mg–Si–Cu alloys results in the segregation of Ag at semi-coherent interfaces of QP2 precipitate.

4 Final Comments

Despite being lightweight and having good strength, the aluminium alloys suffered a bottleneck since they could not have good strength above 150 °C. A race to develop new dilute aluminium alloys with transition metals still cannot compete with the existing commercial alloys in terms of strength. However, minor addition of the transition elements can be adopted to develop a new-generation aluminium alloy. In the last three to four years, ordered precipitates and segregation of a small amount of transition elements at the precipitate–matrix interface attracted attention. Although we presented a brief account of this, there may be other opportunities, including multi-element alloys with newer properties for high performance and newer defects and microstructural architectures through newer processing routes like additive manufacturing. Thus, the research on aluminium alloys will continue to generate interest and excitement.

Acknowledgements The authors received sustained funding from the Department of Science & Technology and Boeing Corporations to research this area. One of the authors (KC) thanks the Science and Engineering Research Board (SERB) of the Government of India for a distinguished fellowship for sustaining this work.

References

1. Gerold V, On the structures of Guinier-Preston zones in Al-Cu alloys introductory paper, *Scr. Metall.* 22 (1988) 927–932. https://doi.org/https://doi.org/10.1016/S0036-9748(88)80077-2.
2. Wang S, Fan C, Crystal Structures of Al_2Cu Revisited: Understanding Existing Phases and Exploring Other Potential Phases, *Metals* (Basel). 9 (2019). https://doi.org/https://doi.org/10.3390/met9101037.
3. Villars P, Cenzual K, eds., *Al_3Sc (ScAl3 rt) Crystal Structure: Datasheet from "PAULING FILE Multinaries Edition – 2012"* in SpringerMaterials https://materials.springer.com/isp/crystallographic/docs/sd_1922024.
4. Knipling KE, Dunand DC, Seidman DN, Criteria for developing castable, creep-resistant aluminum-based alloys - A review, *Int. J. Mater. Res.* 97 (2006) 246–265. https://doi.org/https://doi.org/10.3139/146.101249.
5. Zandbergen HW, Andersen SJ, Jansen J, Structure Determination of Mg_5Si_6 Particles in Al by Dynamic Electron Diffraction Studies, *Science* 277 (1997) 1221–1225. https://doi.org/https://doi.org/10.1126/science.277.5330.1221.
6. Jacobs MH, The structure of the metastable precipitates formed during ageing of an Al-Mg-Si alloy, *Philos. Mag.* 26 (1972) 1–13. https://doi.org/https://doi.org/10.1080/14786437208221015.
7. Andersen SJ, Marioara CD, Vissers R, Frøseth A, Zandbergen HW, The structural relation between precipitates in Al-Mg-Si alloys, the Al-matrix and diamond silicon, with emphasis on the trigonal phase U1-$MgAl_2Si_2$, *Mater. Sci. Eng. A.* 444 (2007) 157–169. https://doi.org/https://doi.org/10.1016/j.msea.2006.08.084.
8. Andersen SJ, Marioara CD, Frøseth A, Vissers R, Zandbergen HW, Crystal structure of the orthorhombic U2-$Al_4Mg_4Si_4$ precipitate in the Al–Mg–Si alloy system and its relation to the β′ and β″ phases, *Mater. Sci. Eng. A.* 390 (2005) 127–138. https://doi.org/https://doi.org/10.1016/j.msea.2004.09.019.
9. Matsuda K, Sakaguchi Y, Miyata Y, Uetani Y ….& Ikeno S, Precipitation sequence of various kinds of metastable phases in Al-1.0mass% Mg2Si-0.4mass% Si alloy, *J. Mater. Sci.* 35 (2000) 179–189. https://doi.org/https://doi.org/10.1023/A:1004769305736.
10. Chakrabarti DJ, Laughlin DE, Phase relations and precipitation in Al-Mg-Si alloys with Cu additions, *Prog. Mater. Sci.* 49 (2004) 389–410. https://doi.org/https://doi.org/10.1016/S0079-6425(03)00031-8.
11. Marioara CD, Andersen SJ, Stene TN, Hasting H, ….& Holmestad R, The effect of Cu on precipitation in Al-Mg-Si alloys, *Philos. Mag.* 87 (2007) 3385–3413. https://doi.org/https://doi.org/10.1080/14786430701287377.
12. Cayron C, Sagalowicz L, Sagalowicz L, Buffat PA, Structural phase transition in Al-Cu-Mg-Si alloys by transmission electron microscopy study on an Al-4 wt% Cu-1 wt% Mg-Ag alloy reinforced by SiC particles, Philos. Mag. A 79 (1999) 2833–2851. https://doi.org/https://doi.org/10.1080/01418619908212027.
13. Matsuda K, Ikeno S, Uetani Y, Sato T, Metastable phases in an Al-Mg-Si alloy containing copper, *Metall. Mater. Trans. A.* 32 (2001) 1293–1299. https://doi.org/https://doi.org/10.1007/s11661-001-0219-2.
14. Arnberg L, Aurivillius B, Wahlström E, Malmros G ….& Sukhoverkhov VF, The Crystal Structure of Al(x)Cu2Mg(12-x)Si7, (h-AlCuMgSi)., *Acta Chem. Scand.* 34a (1980) 1–5. https://doi.org/https://doi.org/10.3891/acta.chem.scand.34a-0001.
15. Wolverton C, Crystal structure and stability of complex precipitate phases in Al-Cu-Mg-(Si) and Al-Zn-Mg alloys, *Acta Mater.* 49 (2001) 3129–3142. https://doi.org/https://doi.org/10.1016/S1359-6454(01)00229-4.
16. Berg LK, Gjønnes J, Hansen V, Li XZ ….& Wallenberg LR, GP-zones in Al-Zn-Mg alloys and their role in artificial aging, *Acta Mater.* 49 (2001) 3443–3451. https://doi.org/https://doi.org/10.1016/S1359-6454(01)00251-8.
17. Nie J F, in: *Phys. Metall.*, Elsevier (2014), p 2009. https://doi.org/10.1016/B978-0-444-53770-6.00020-4.
18. Biswas A, Siegel DJ, Wolverton C, Seidman DN, Precipitates in Al-Cu alloys revisited: Atom-probe tomographic experiments and first-principles calculations of compositional evolution and interfacial segregation, *Acta Mater.* 59 (2011) 6187–6204. https://doi.org/https://doi.org/10.1016/j.actamat.2011.06.036.
19. Konno TJ, Hiraga K, Kawasaki M, Guinier-Preston (GP) zone revisited: atomic level observation by HAADF-TEM technique, *Scr. Mater.* 44 (2001) 2303–2307. https://doi.org/https://doi.org/10.1016/S1359-6462(01)00909-5.
20. Chung TF, Yang YL, Hsiao CN, Li WC, ….& Yang JR, Morphological evolution of GP zones and nanometer-sized precipitates in the AA2050 aluminium alloy, *Int. J. Light.*

Mater. Manuf. 1 (2018) 142–156. https://doi.org/https://doi.org/10.1016/j.ijlmm.2018.06.002.
21. Bansal U, Development of a coarsening resistant microstructure in precipitation strengthened aluminium alloys with Zr, Ta and Hf, Indian Institute of Science, (2021), p 200.
22. Sankaran R, Laird C, Interfacial structure of plate-like precipitates, *Philos. Mag.* 29 (1974) 179–215. https://doi.org/https://doi.org/10.1080/14786437408213562.
23. Ardell AJ, Precipitation hardening, *Metall. Trans. A.* 16 (1985) 2131–2165. https://doi.org/https://doi.org/10.1007/BF02670416.
24. Zhu AW, Starke EA, Strengthening effect of unshearable particles of finite size: a computer experimental study, *Acta Mater.* 47 (1999) 3263–3269. https://doi.org/https://doi.org/10.1016/S1359-6454(99)00179-2.
25. Song M, He Y, Fang S, Effects of Zr Content on the Yield Strength of an Al-Sc Alloy, *J. Mater. Eng. Perform.* 20 (2011) 377–381. https://doi.org/https://doi.org/10.1007/s11665-010-9693-2.
26. Gao Z, Li H, Lai Y, Ou Y, Li D, Effects of minor Zr and Er on microstructure and mechanical properties of pure aluminum, *Mater. Sci. Eng. A.* 580 (2013) 92–98. https://doi.org/https://doi.org/10.1016/j.msea.2013.05.035.
27. Makineni SK, Sugathan S, Meher S, Banerjee R, ….&, Chattopadhyay K, Enhancing elevated temperature strength of copper containing aluminium alloys by forming $L1_2$ Al_3Zr precipitates and nucleating θ″ precipitates on them, *Sci. Rep.* 7 (2017) 1–9. https://doi.org/https://doi.org/10.1038/s41598-017-11540-2.
28. Mondol S, Makineni SK, Kumar S, Chattopadhyay K, Enhancement of High Temperature Strength of 2219 Alloys Through Small Additions of Nb and Zr and a Novel Heat Treatment, Metall. Mater. Trans. A Phys. Metall. Mater. Sci. 49 (2018) 3047–3057. https://doi.org/https://doi.org/10.1007/s11661-018-4614-3.
29. Hatch J E, *Aluminum: Properties and Physical Metallurgy*, Aluminum Association Inc. and ASM International, (1984), p 424, ISBN: 978-0-87170-176-3.
30. Kharakterova ML, Eskin DG, Toropova LS, Precipitation hardening in ternary alloys of the Al-Sc-Cu and Al-Sc-Si systems, *Acta Metall. Mater.* 42 (1994) 2285–2290. https://doi.org/https://doi.org/10.1016/0956-7151(94)90307-7.
31. Gao YH, Guan PF, Su R, Chen HW, ….& Ma E, Segregation-sandwiched stable interface suffocates nanoprecipitate coarsening to elevate creep resistance, *Mater. Res. Lett.* 8 (2020) 446–453. https://doi.org/https://doi.org/10.1080/21663831.2020.1799447.
32. Chen BA, Pan L, Wang RH, Liu G, ….& Sun J, Effect of solution treatment on precipitation behaviors and age hardening response of Al-Cu alloys with Sc addition, *Mater. Sci. Eng. A.* 530 (2011) 607–617. https://doi.org/https://doi.org/10.1016/j.msea.2011.10.030.
33. Gao YH, Cao LF, Kuang J, Zhang JY, ….& Sun J, Dual effect of Cu on the Al_3Sc nanoprecipitate coarsening, *J. Mater. Sci. Technol.* 37 (2020) 38–45. https://doi.org/https://doi.org/10.1016/j.jmst.2019.07.035.
34. Chen BA, Liu G, Wang RH, Zhang JY ….& Sun J, Effect of interfacial solute segregation on ductile fracture of Al-Cu-Sc alloys, *Acta Mater.* 61 (2013) 1676–1690. https://doi.org/https://doi.org/10.1016/j.actamat.2012.11.043.
35. Liu C, Teng G, Ma Z, Wei L, ….& Chen Y, Effects of Sc and Zr microalloying on the microstructure and mechanical properties of high Cu content 7xxx Al alloy, *Int. J. Miner. Metall. Mater.* 26 (2019) 1559–1569. https://doi.org/https://doi.org/10.1007/s12613-019-1840-7.
36. Lee SL, Wu CT, Chen TD, Effects of Minor Sc and Zr on the Microstructure and Mechanical Properties of Al-4.6Cu-0.3Mg-0.6Ag Alloys, *J. Mater. Eng. Perform.* 24 (2015) 1165–1172. https://doi.org/https://doi.org/10.1007/s11665-014-1364-2.
37. Yang C, Cao L, Gao Y, Cheng P, ….& Sun J, Nanostructural Sc-based hierarchy to improve the creep resistance of Al–Cu alloys, *Mater. Des.* 186 (2020) 108309. https://doi.org/https://doi.org/10.1016/j.matdes.2019.108309.
38. Yang C, Zhang P, Shao D, Wang RH, ….& Sun J, The influence of Sc solute partitioning on the microalloying effect and mechanical properties of Al-Cu alloys with minor Sc addition, *Acta Mater.* 119 (2016) 68–79. https://doi.org/https://doi.org/10.1016/j.actamat.2016.08.013.
39. Nasim W, Yazdi S, Santamarta R, Malik J ….& Karaman I, Structure and growth of core–shell nanoprecipitates in Al–Er–Sc–Zr–V–Si high-temperature alloys, *J. Mater. Sci.* 54 (2019) 1857–1871. https://doi.org/https://doi.org/10.1007/s10853-018-2941-9.
40. Xu W, Guoqin C, Bing LI, Lianmei WU, Daming J, Effects of Sc, Zr and Ti on the microstructure and properties of Al alloys with high Mg content. *Rare Metals* 29, 66–71 (2010). https://doi.org/https://doi.org/10.1007/s12598-010-0012-8.
41. Van Dalen M E, Dunand D C, Seidman D N, in *Affordable Metal Matrix Composites for High Performance Applications II* (eds) Pandey A B, Kendig K L, Lewandowski J J, Shah S S, (2003), p 195.
42. Jiang L, Rouxel B, Langan T, Dorin T, Coupled segregation mechanisms of Sc, Zr and Mn at θ′ interfaces enhances the strength and thermal stability of Al-Cu alloys, *Acta Mater.* 206 (2021) 116634. https://doi.org/https://doi.org/10.1016/j.actamat.2021.116634.
43. Rouxel B, M. Ramajayam M, Langan TJ, Lamb J ….& Dorin T, Effect of dislocations, $Al_3(Sc,Zr)$ distribution and ageing temperature on θ′ precipitation in Al-Cu-(Sc)-(Zr) alloys, *Materialia*. 9 (2020). https://doi.org/https://doi.org/10.1016/j.mtla.2020.100610.
44. Dorin T, Ramajayam M, Lamb J, Langan T, Effect of Sc and Zr additions on the microstructure/strength of Al-Cu binary alloys, *Mater. Sci. Eng. A.* 707 (2017) 58–64. https://doi.org/https://doi.org/10.1016/j.msea.2017.09.032.
45. Gao YH, Cao LF, Kuang J, Zhang JY, ….& Sun J, Assembling dual precipitates to improve high-temperature resistance of multi-microalloyed Al–Cu alloys, *J. Alloys Compd.* 822 (2020) 153629. https://doi.org/https://doi.org/10.1016/j.jallcom.2019.153629.
46. Mondol S, Alam T, Banerjee R, Kumar S, Chattopadhyay K, Development of a high temperature high strength Al alloy by addition of small amounts of Sc and Mg to 2219 alloy, *Mater. Sci. Eng. A.* 687 (2017) 221–231. https://doi.org/https://doi.org/10.1016/j.msea.2017.01.037.
47. Mondol S, Kashyap S, Kumar S, Chattopadhyay K, Improvement of high temperature strength of 2219 alloy by Sc and Zr addition through a novel three-stage heat treatment route, *Mater. Sci. Eng. A.* 732 (2018) 157–166. https://doi.org/https://doi.org/10.1016/j.msea.2018.07.003.
48. Pan S, Chen X, Zhou X, Wang Z ….& Li S, Micro-alloying effect of Er and Zr on microstructural evolution and yield strength of Al-3Cu (wt.%) binary alloys, *Mater. Sci. Eng. A.* 790 (2020) 139391. https://doi.org/https://doi.org/10.1016/j.msea.2020.139391.
49. Bryant JD, The effects of preaging treatments on aging kinetics and mechanical properties in AA6111 aluminum autobody sheet, *Metall Mater Trans A* 30, 1999–2006 (1999). https://doi.org/https://doi.org/10.1007/s11661-999-0010-3.
50. Aruga Y, Kozuka M, Takaki Y, Sato T, Effects of natural aging after pre-aging on clustering and bake-hardening behavior in an Al-Mg-Si alloy, *Scr. Mater.* 116 (2016) 82–86. https://doi.org/https://doi.org/10.1016/j.scriptamat.2016.01.019.

51. Pogatscher S, Antrekowitsch H, Leitner H, Pöschmann D ….& Uggowitzer PJ, Influence of interrupted quenching on artificial aging of Al-Mg-Si alloys, *Acta Mater.* 60 (2012) 4496–4505. https://doi.org/https://doi.org/10.1016/j.actamat.2012.04.026.
52. Mørtsell EA, Marioara CD, Andersen SJ, Ringdalen IG ….& Holmestad R, The effects and behaviour of Li and Cu alloying agents in lean Al-Mg-Si alloys, *J. Alloys Compd.* 699 (2017) 235–242. https://doi.org/https://doi.org/10.1016/j.jallcom.2016.12.273.
53. Mørtsell EA, Andersen SJ, Friis J, Marioara CD, Holmestad R, Atomistic details of precipitates in lean Al–Mg–Si alloys with trace additions of Ag and Ge studied by HAADF-STEM and DFT, *Philos. Mag.* 97 (2017) 851–866. https://doi.org/https://doi.org/10.1080/14786435.2017.1281461.
54. Ding L, Hu H, Jia Z, Weng Y ….& Liu Q, The disordered structure of Q′ and C phases in Al-Mg-Si-Cu alloy, *Scr. Mater.* 118 (2016) 55–59. https://doi.org/https://doi.org/10.1016/j.scriptamat.2016.03.011.
55. Ding L, Jia Z, Nie JF, Weng Y ….& Liu Q, The structural and compositional evolution of precipitates in Al-Mg-Si-Cu alloy, *Acta Mater.* 145 (2018) 437–450. https://doi.org/https://doi.org/10.1016/j.actamat.2017.12.036.
56. Qian F, Mørtsell EA, Marioara CD, Andersen SJ, Li Y, Improving ageing kinetics and precipitation hardening in an Al-Mg-Si alloy by minor Cd addition, *Materialia.* 4 (2018) 33–37. https://doi.org/https://doi.org/10.1016/j.mtla.2018.09.006.
57. Kim JH, Marioara CD, Holmestad R, Kobayashi E, SatoT, Effects of Cu and Ag additions on age-hardening behavior during multi-step aging in Al-Mg-Si alloys, *Mater. Sci. Eng. A.* 560 (2013) 154–162. https://doi.org/https://doi.org/10.1016/j.msea.2012.09.051.
58. Wenner S, Marioara CD, Ramasse QM, Kepaptsoglou DM ….& Holmestad R, Atomic-resolution electron energy loss studies of precipitates in an Al-Mg-Si-Cu-Ag alloy, *Scr. Mater.* 74 (2014) 92–95. https://doi.org/https://doi.org/10.1016/j.scriptamat.2013.11.007.
59. Marioara CD, Nakamura J, Matsuda K, Andersen SJ ….& Ikeno S, HAADF-STEM study of β-type precipitates in an over-aged Al-Mg-Si-Ag alloy, *Philos. Mag.* 92 (2012) 1149–1158. https://doi.org/https://doi.org/10.1080/14786435.2011.642319.
60. Saito T, Wenner S, Osmundsen E, Marioara CD ….& Holmestad R, The effect of Zn on precipitation in Al-Mg-Si alloys, *Philos. Mag.* 94 (2014) 2410–2425. https://doi.org/https://doi.org/10.1080/14786435.2014.913819.
61. Polmear IJ, Pons G, Barbaux Y, Octor H ….& Rogers S, After Concorde: Evaluation of creep resistant Al-Cu-Mg-Ag alloys, *Mater. Sci. Technol.* 15 (1999) 861–868. https://doi.org/https://doi.org/10.1179/026708399101506599.
62. Weng Y, Ding L, Zhang Z, Jia Z ….& Liu Q, Effect of Ag addition on the precipitation evolution and interfacial segregation for Al–Mg–Si alloy, *Acta Mater.* 180 (2019) 301–316. https://doi.org/https://doi.org/10.1016/j.actamat.2019.09.015.
63. Sunde JK, Lu F, Marioara CD, Holmedal B, Holmestad R, Linking mechanical properties to precipitate microstructure in three Al-Mg-Si(-Cu) alloys, *Mater. Sci. Eng. A.* 807 (2021). https://doi.org/https://doi.org/10.1016/j.msea.2021.140862.
64. Kwon EP, Woo KD, Kim SH, Kang DS ….& Jeon JY, The effect of an addition of Sc and Zr on the precipitation behavior of AA6061 alloy, *Met. Mater. Int.* 16 (2010) 701–707. https://doi.org/https://doi.org/10.1007/s12540-010-1002-y.
65. Nakamura T, Matsuo T, Ikeda M, Komatsu SY, Effect of scandium addition on aging behavior of 6061 aluminum alloy, *Adv. Mater. Res.* 15–17 (2007) 7–12. https://doi.org/https://doi.org/10.4028/www.scientific.net/amr.15-17.7.
66. Vlach M, Smola B, Stulíková I, Očenášek V, Microstructure and mechanical properties of the AA6082 aluminium alloy with small additions of Sc and Zr, *Int. J. Mater. Res.* 100 (2009) 420–423. https://doi.org/https://doi.org/10.3139/146.110022.
67. Rokhlin LL, Bochvar NR, Tarytina IE, Joint effect of scandium and zirconium on the structure and the strength properties of Al–Mg_2Si–Based alloys, *Russ. Metall.* 2015 (2015) 726–731. https://doi.org/https://doi.org/10.1134/S0036029515090116.
68. Lityńska-Dobrzyńska L, Dutkiewicz J, Maziarz W, Ochin P, Structure and properties of Al-Mg-Si alloys with Zr and Sc additions produced by melt spinning and twin rolling casting techniques, *Kov. Mater.* 48 (2010) 9–15. https://doi.org/https://doi.org/10.4149/km_2010_1_9.
69. Lityńska-Dobrzyńska L, Precipitation of phases in Al-Mg-Si-Cu alloy with Sc and Zr additions during heat treatment, *Solid State Phenom.* 130 (2007) 163–166. https://doi.org/https://doi.org/10.4028/www.scientific.net/SSP.130.163.
70. Han J, Woo KD, Lee KJ, Chen Y, Effect of step quenching and Zr addition on the microstructure and mechanical properties of Al-Mg-Si alloy, *J. Korean Inst. Met. Mater.* 52 (2014) 173–179. https://doi.org/https://doi.org/10.3365/KJMM.2014.52.2.101.
71. Babaniaris S, Ramajayam M, Jiang L, Langan T, Dorin T, Tailored precipitation route for the effective utilisation of Sc and Zr in an Al-Mg-Si alloy, *Materialia.* 10 (2020) 100656. https://doi.org/https://doi.org/10.1016/j.mtla.2020.100656.
72. Huda Z, Edi P, Materials selection in design of structures and engines of supersonic aircrafts: A review, *Mater. Des.* 46 (2013) 552–560. https://doi.org/https://doi.org/10.1016/j.matdes.2012.10.001.
73. Liu JZ, Chen JH, Yang XB, Ren S….& Zou J, Revisiting the precipitation sequence in Al-Zn-Mg-based alloys by high-resolution transmission electron microscopy, *Scr. Mater.* 63 (2010) 1061–1064. https://doi.org/https://doi.org/10.1016/j.scriptamat.2010.08.001.
74. Chen Z, Yan K, Ren C, Naseem S, Precipitation sequence and hardening effect in 7A85 aluminum alloy, *J. Alloys Compd.* 875 (2021) 159950. https://doi.org/https://doi.org/10.1016/j.jallcom.2021.159950.
75. Sha G, Cerezo A, Early-stage precipitation in Al-Zn-Mg-Cu alloy (7050), *Acta Mater.* 52 (2004) 4503–4516. https://doi.org/https://doi.org/10.1016/j.actamat.2004.06.025.
76. Buha J, Lumley RN, Crosky AG, Secondary ageing in an aluminium alloy 7050, *Mater. Sci. Eng. A.* 492 (2008) 1–10. https://doi.org/https://doi.org/10.1016/j.msea.2008.02.039.
77. Liu D, Xiong B, Bian F, Li Z ….& Liu H, Quantitative study of nanoscale precipitates in Al-Zn-Mg-Cu alloys with different chemical compositions, *Mater. Sci. Eng. A.* 639 (2015) 245–251. https://doi.org/https://doi.org/10.1016/j.msea.2015.04.104.
78. Lou SM, Qu CD, Guo GX, Ran LW ….& Wang QB. Effect of Fabrication Parameters on the performance of 0.5 wt.% Graphene Nanoplates-Reinforced Aluminum Composites. *Materials.* 13 (2020) 3483. https://doi.org/https://doi.org/10.3390/ma13163483
79. Meng X, Zhang D, Zhang W, Qiu C ….& Chen J, Microstructure and mechanical properties of a high-Zn aluminum alloy prepared by melt spinning and extrusion, *J. Alloys Compd.* 819 (2020) 152990. https://doi.org/https://doi.org/10.1016/j.jallcom.2019.152990.
80. Meng X, Zhang D, Zhang W, Qiu C ….& Chen J, Microstructure and mechanical properties of a rapidly-solidified and extruded Al-13.2Zn-2.5Mg-1.2Cu-0.2Zr alloy and its aging hardening response at 120 °C, *Mater. Sci. Eng. A.* 826 (2021). https://doi.org/https://doi.org/10.1016/j.msea.2021.141969.
81. Won SJ, So H, Kang L, Oh SJ, Kim KH, Development of a high-strength Al-Zn-Mg-Cu-based alloy via multi-strengthening mechanisms, *Scr. Mater.* 205 (2021) 114216. https://doi.org/https://doi.org/10.1016/j.scriptamat.2021.114216.

82. Lee SH, Jung JG, Baik SI, Park SH ….& Euh K, Effects of Ti addition on the microstructure and mechanical properties of Al–Zn–Mg–Cu–Zr alloy, *Mater. Sci. Eng. A.* 801 (2021) 140437. https://doi.org/https://doi.org/10.1016/j.msea.2020.140437.
83. Shi C, Chen XG, Effect of vanadium on hot deformation and microstructural evolution of 7150 aluminum alloy, *Mater. Sci. Eng. A.* 613 (2014) 91–102. https://doi.org/https://doi.org/10.1016/j.msea.2014.06.082.
84. Ying T, Gu L, Tang X, Wang J, Zeng X, Effect of Sc microalloying on microstructure evolution and mechanical properties of extruded Al–Zn–Mg–Cu alloys, *Mater. Sci. Eng. A.* 831 (2021) 142197. https://doi.org/https://doi.org/10.1016/j.msea.2021.142197.
85. Shi C, Chen XG, Effect of Zr addition on hot deformation behavior and microstructural evolution of AA7150 aluminum alloy, *Mater. Sci. Eng. A.* 596 (2014) 183–193. https://doi.org/https://doi.org/10.1016/j.msea.2013.12.057.
86. Guo Z, Zhao G, Chen XG, Effects of two-step homogenization on precipitation behavior of Al3Zr dispersoids and recrystallization resistance in 7150 aluminum alloy, *Mater. Charact.* 102 (2015) 122–130. https://doi.org/https://doi.org/10.1016/j.matchar.2015.02.016.
87. Chen K, Tang J, Jiang F, Teng J ….& Zhang H, The role of various Zr additions in static softening behavior of Al-Zn-Mg-Cu alloys during interval holding of double-stage hot deformation, *J. Alloys Compd.* 792 (2019) 1112–1121. https://doi.org/https://doi.org/10.1016/j.jallcom.2019.04.090.
88. Curle UA, Cornish LA, Govender G, Predicting yield strengths of Al-Zn-Mg-Cu-(Zr) aluminium alloys based on alloy composition or hardness, *Mater. Des.* 99 (2016) 211–218. https://doi.org/https://doi.org/10.1016/j.matdes.2016.03.071.
89. Zhang M, Liu T, He C, Ding J ….& Zhao N, Evolution of microstructure and properties of Al-Zn-Mg-Cu-Sc-Zr alloy during aging treatment, *J. Alloys Compd.* 658 (2016) 946–951. https://doi.org/https://doi.org/10.1016/j.jallcom.2015.10.296.
90. Senkov ON, Shagiev MR, Senkova SV, Miracle DB, Precipitation of Al_3(Sc,Zr) particles in an Al-Zn-Mg-Cu-Sc-Zr alloy during conventional solution heat treatment and its effect on tensile properties, *Acta Mater.* 56 (2008) 3723–3738. https://doi.org/https://doi.org/10.1016/j.actamat.2008.04.005.
91. Deng Y, Yin Z, Zhao K, Duan J, He Z, Effects of Sc and Zr microalloying additions on the microstructure and mechanical properties of new Al-Zn-Mg alloys, *J. Alloys Compd.* 530 (2012) 71–80. https://doi.org/https://doi.org/10.1016/j.jallcom.2012.03.108.
92. Deng Y, Yin Z, Zhao K, Duan J ….& He Z, Effects of Sc and Zr microalloying additions and aging time at 120°C on the corrosion behaviour of an Al-Zn-Mg alloy, *Corros. Sci.* 65 (2012) 288–298. https://doi.org/https://doi.org/10.1016/j.corsci.2012.08.024.
93. Li B, Pan Q, Chen C, Wu H, Yin Z, Effects of solution treatment on microstructural and mechanical properties of Al-Zn-Mg alloy by microalloying with Sc and Zr, *J. Alloys Compd.* 664 (2016) 553–564. https://doi.org/https://doi.org/10.1016/j.jallcom.2016.01.016.
94. Liu J, Yao P, Zhao N, Shi C ….& Yang S, Effect of minor Sc and Zr on recrystallization behavior and mechanical properties of novel Al-Zn-Mg-Cu alloys, *J. Alloys Compd.* 657 (2016) 717–725. https://doi.org/https://doi.org/10.1016/j.jallcom.2015.10.122.
95. Xiao QF, Huang JW, Jiang YG, Jiang FQ ….& Xu GF, Effects of minor Sc and Zr additions on mechanical properties and microstructure evolution of Al−Zn−Mg−Cu alloys, *Trans. Nonferrous Met. Soc. China* (English Ed. 30 (2020) 1429–1438. https://doi.org/https://doi.org/10.1016/S1003-6326(20)65308-0.
96. Wang K, Yin D, Zhao YC, Atrens A, Zhao MC, Microstructural evolution upon heat treatments and its effect on corrosion in Al-Zn-Mg alloys containing Sc and Zr, *J. Mater. Res. Technol.* 9 (2020) 5077–5089. https://doi.org/https://doi.org/10.1016/j.jmrt.2020.03.025.
97. Deng Y, Yin Z, Duan J, Zhao K ….& He Z, Evolution of microstructure and properties in a new type 2 mm Al-Zn-Mg-Sc-Zr alloy sheet, *J. Alloys Compd.* 517 (2012) 118–126. https://doi.org/https://doi.org/10.1016/j.jallcom.2011.12.049.
98. Milligan BK, Roy S, Hawkins CS, Allard LF, Shyam A, Impact of microstructural stability on the creep behavior of cast Al–Cu alloys, *Mater. Sci. Eng. A.* 772 (2020) 138697. https://doi.org/https://doi.org/10.1016/j.msea.2019.138697.
99. Roy S, Allard LF, Rodriguez A, Porter WD, Shyam A, Comparative Evaluation of Cast Aluminum Alloys for Automotive Cylinder Heads: Part II—Mechanical and Thermal Properties, *Metall. Mater. Trans. A.* 48 (2017) 2543–2562. https://doi.org/https://doi.org/10.1007/s11661-017-3986-0.
100. Bahl S, Xiong L, Allard LF, Michi RA ….& Shyam A, Aging behavior and strengthening mechanisms of coarsening resistant metastable θ' precipitates in an Al–Cu alloy, *Mater. Des.* 198 (2021) 109378. https://doi.org/https://doi.org/10.1016/j.matdes.2020.109378.
101. Gao YH, Yang C, Zhang JY, Cao LF ….& Ma E, Stabilizing nanoprecipitates in Al-Cu alloys for creep resistance at 300°C, *Mater. Res. Lett.* 7 (2019) 18–25. https://doi.org/https://doi.org/10.1080/21663831.2018.1546773.
102. Shyam A, Roy S, Shin D, Poplawsky JD ….& Haynes JA, Elevated temperature microstructural stability in cast AlCuMnZr alloys through solute segregation, *Mater. Sci. Eng. A.* 765 (2019) 138279. https://doi.org/https://doi.org/10.1016/j.msea.2019.138279.
103. Ding J, Cui C, Sun Y, Zhao L, Cui S, Effect of Mo, Zr, and Y on the high-temperature properties of Al-Cu-Mn alloy, *J. Mater. Res.* 34 (2019) 3853–3861. https://doi.org/https://doi.org/10.1557/jmr.2019.288.
104. Gao YH, Kuang J, Zhang JY, Liu G, Sun J, Tailoring precipitation strategy to optimize microstructural evolution, aging hardening and creep resistance in an Al–Cu–Sc alloy by isochronal aging, *Mater. Sci. Eng. A.* 795 (2020) 139943. https://doi.org/https://doi.org/10.1016/j.msea.2020.139943.
105. Jiang L, Li JK, Liu G, Wang RH ….& Cao XZ, Length-scale dependent microalloying effects on precipitation behaviors and mechanical properties of Al-Cu alloys with minor Sc addition, *Mater. Sci. Eng. A.* 637 (2015) 139–154. https://doi.org/https://doi.org/10.1016/j.msea.2015.04.035.
106. Poplawsky JD, Milligan BK, Allard LF, Shin D ….& Shyam A, The synergistic role of Mn and Zr/Ti in producing θ′/$L1_2$ co-precipitates in Al-Cu alloys, *Acta Mater.* 194 (2020) 577–586. https://doi.org/https://doi.org/10.1016/j.actamat.2020.05.043.
107. Matsuda K, Teguri D, Uetani Y, Sato T, Ikeno S, Cu-segregation at the Q′/α-Al interface in Al-Mg-Si-Cu alloy, *Scr. Mater.* 47 (2002) 833–837. https://doi.org/https://doi.org/10.1016/S1359-6462(02)00325-1.
108. Weng Y, Jia Z, Ding L, Du K ….& Wu X, Special segregation of Cu on the habit plane of lath-like β′ and QP2 precipitates in Al-Mg-Si-Cu alloys, *Scr. Mater.* 151 (2018) 33–37. https://doi.org/https://doi.org/10.1016/j.scriptamat.2018.03.032.
109. Weng Y, Jia Z, Ding L, Muraishi S ….& Liu Q, The multiple orientation relationships and morphology of β' phase in Al-Mg-

Si-Cu alloy, *J. Alloys Compd.* 767 (2018) 81–89. https://doi.org/https://doi.org/10.1016/j.jallcom.2018.07.077.
110. Jin M, Li J, Shao GJ, Study of Cu Addition on Precipitation Behaviors and Mechanical Properties in AA6082 Al-Mg-Si Alloy, *Mater. Sci. Forum.* 546–549 (2007) 825–828. https://doi.org/https://doi.org/10.4028/www.scientific.net/msf.546-549.825.
111. Weng Y, Ding L, Jia Z, Liu Q, Effect of combined addition of Ag and Cu on the precipitation behavior for an Al-Mg-Si alloy, *Mater. Charact.* 171 (2021) 110736. https://doi.org/https://doi.org/10.1016/j.matchar.2020.110736.